Inelastically decoupling dark matter

Ronny Frumkin,[1,2] Yonit Hochberg,[1,3] Eric Kuflik,[1,3] and Binyamin Vilk[1]
[1]*Racah Institute of Physics, Hebrew University of Jerusalem, Jerusalem 91904, Israel*
[2]*Department of Particle Physics and Astrophysics, Weizmann Institute of Science, Rehovot 7610001, Israel*
[3]*Laboratory for Elementary Particle Physics, Cornell University, Ithaca, New York 14853, USA*

(Received 7 September 2025; accepted 18 December 2025; published 6 January 2026)

We present a new dark matter candidate, the inelastically decoupling relic (iELDER), which is a cold thermal relic whose abundance is determined by the freeze out of its inelastic scattering off of bath particles in the presence of $3 \to 2$ self-annihilations. The dark matter is predicted to be light, in the $\mathcal{O}(\mathrm{MeV} - \mathrm{GeV})$ range, with significant self-annihilations and very weak inelastic couplings to ordinary matter. We demonstrate iELDER dark matter using a Z_3-symmetric toy model as well as quantum chromodynamics (QCD)-like pion theories—the latter showing promising prospects for detection and providing a new benchmark for future searches.

DOI: 10.1103/52fd-b266

I. INTRODUCTION

For decades, indirect evidence for the existence of dark matter (DM) has accumulated, however its particle identity remains unknown. Much theoretical and experimental effort has focused on exploring DM as a thermal relic of the early universe. The most well-studied thermal relic is the weakly interacting massive particle (WIMP) scenario, which suggests the DM relic abundance is set by the freeze-out of a $2 \to 2$ annihilation process. Experimental exclusion of much of the natural WIMP parameter space has spurred recent works suggesting alternatives to the WIMP (such as Refs. [1–17]; for recent reviews, see Refs. [18,19]). Among these ideas are coscattering DM [11], strongly interacting massive particles (SIMPs) [5,6] and elastically decoupling relics (ELDERs) [8,12]. In the first case, the DM relic abundance is determined by the decoupling of an inelastic DM number-changing scattering process off of bath particles, with a slightly heavier bath particle. In the second case, the $3 \to 2$ self-annihilation of DM sets the relic abundance, while an entropy transfer process is open between the dark sector and the bath. In the third case, the DM decouples from the bath while the $3 \to 2$ process is still active, and the relic abundance is controlled by the elastic scattering of the DM off of bath particles.

In this work we combine main elements from these ideas where the elastic scattering process in SIMPs and ELDERs are replaced with an inelastic scattering process. Thus we study a DM candidate with two relevant processes for freeze-out. The first is $3 \to 2$ self-annihilations of DM particles (χ_i),

$$\chi_j \chi_k \chi_\ell \to \chi_m \chi_n. \tag{1}$$

The second is an inelastic scattering of DM into a heavier particle (ψ) off of a Standard Model (SM) bath particle (ϕ), i.e.,

$$\chi_i \phi \leftrightarrow \psi \phi. \tag{2}$$

The particle ψ has its chemical potential kept to zero during DM freeze-out in one of two ways:

(i) ψ has number-changing interactions with the SM bath (such as $\psi\psi \to \mathrm{SM}$); or
(ii) ψ is one of the χ_i participating in the $3 \to 2$ self-annihilations.

In both cases we find a new mechanism of freeze-out where the DM abundance is controlled by the inelastic scattering process in the presence of $3 \to 2$ self-annihilations, which we dub an inelastically decoupling relic, or iELDER. For the latter case (ii), we show that this situation generically arises in SIMP pion models, altering the parameter space. Figure 1 schematically describes the processes involved in setting the relic abundance in both cases and the decoupling hierarchy in the different phases. The top panel matches the first set of assumptions, while the bottom panel relates to the second set. The latter case is illustrated in a quantum chromodynamics (QCD)-like theory, where we identify the dark sector particles χ and ψ as dark pions, as will be discussed below.

This paper is organized as follows. Section II describes a general setup introducing the iELDER DM phase

Published by the American Physical Society under the terms of the Creative Commons Attribution 4.0 International license. Further distribution of this work must maintain attribution to the author(s) and the published article's title, journal citation, and DOI. Funded by SCOAP³.

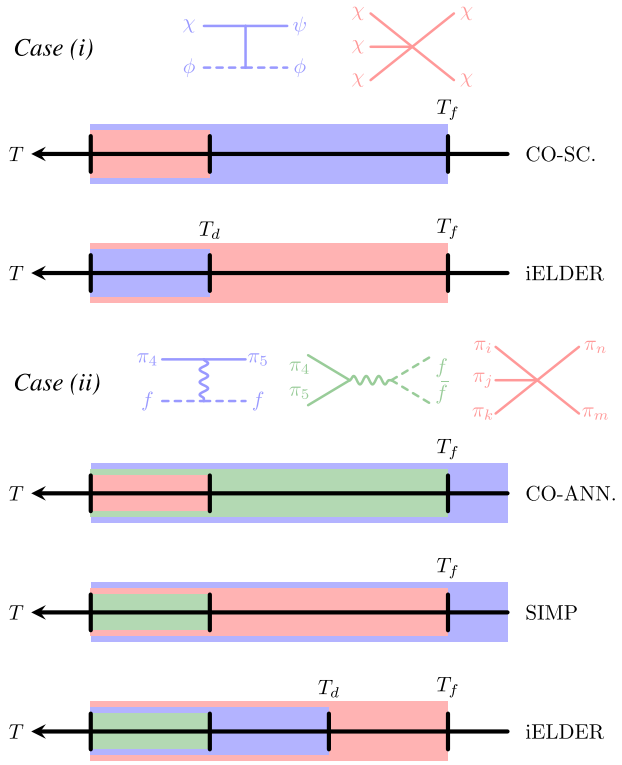


FIG. 1. Schematic setup. Illustration of the iELDER mechanism and other phases in a general setup (case (i), top panel) and a QCD-like pion theory (case (ii), bottom panel). Colored areas represent the epochs when the relevant processes are active. $T_d(T_f)$ denote temperature of decoupling (freeze out). Case (i): ψ is in chemical equilibrium with the bath due to interactions with the SM (such as $\psi\psi \to$ SM). Two regimes emerge: iELDER and coscattering, depending on the order in which the processes decouple. Case (ii): ψ is one of the dark particles participating in the $3 \to 2$ process, resulting in three distinct regimes of coannihilation, SIMP or iELDER, depending on the order in which the processes decouple. We illustrate this scenario via a QCD-like theory of dark pions.

[demonstrated via case (i)], including the relevant Boltzmann equations. Section III presents a toy model that realizes this scenario. Section IV presents the iELDER phase in a QCD-like pion model according to the assumptions of case (ii). We conclude in Sec. V.

II. THE IELDER PHASE

First we take a general model-independent approach to introduce an iELDER DM phase, under the assumptions of case (i). Consider a DM candidate χ with mass m_χ and a heavier dark particle ψ of mass $m_\psi = m_\chi(1+\Delta)$, where the particles undergo inelastic scattering with a relativistic bath particle ϕ, $\chi\phi \leftrightarrow \psi\phi$. The χ particles also undergo self-interactions via a $3 \to 2$ annihilation process, $\chi\chi\chi \leftrightarrow \chi\chi$.

We consider the case where ψ is chemically coupled to the bath at all times through the process $\psi\psi \leftrightarrow \phi\phi$, and the process $\chi\chi \leftrightarrow \psi\psi$ is absent or negligible. The annihilation process $\chi\psi \leftrightarrow \phi\phi$ depends on the Boltzmann-suppressed population of ψ, while the number-changing inelastic scattering process involves the abundant bath particle ϕ, an so the annihilation will always decouple before the inelastic process, and will be neglected as well. At early times, χ is relativistic and remains in equilibrium with the bath. Later, when the bath temperature drops beneath the mass of χ, $T_{\rm bath} < m_\chi$, the χ number density is exponentially suppressed. If the inelastic scattering decouples before the $3 \to 2$ self-annihilations, the DM enters what we denote as the iELDER regime: χ thermally detaches from the bath and then cannibalizes [3], thus cooling down slower than the bath, and so the DM number density drops slower then if it would have been in thermal equilibrium with the SM bath. When the $3 \to 2$ process later decouples, the number density of χ freezes out. Because the number density of χ only mildly changes throughout the cannibalization epoch, its abundance at freeze out—and hence the relic abundance today—is set by the rate of the inelastic process. This is in similar spirit to ELDER DM, though here it is an *inelastic* scattering process that is setting the DM abundance. On the other hand, if the $3 \to 2$ self-annihilations decouple first, DM is in a coscattering regime [11]: the inelastic scattering is the only number-changing process active, and so when it decouples it sets the relic abundance. Overall, in this setup the DM relic abundance is always set by the inelastic process cross section, but through two different phases, corresponding to different coupling strengths.

Having described the setup above, we can now write the two coupled Boltzmann equations for the χ number density n_χ and energy density ρ_χ,

$$\dot{n}_\chi + 3Hn_\chi = -\langle\sigma_{3\to2}v^2\rangle(n_\chi^3 - n_\chi^2 n_\chi^{\rm eq}) - n_\phi^{\rm eq}\langle\sigma_{\chi\to\psi}v\rangle(n_\chi - n_\chi^{\rm eq}), \tag{3}$$

and

$$\dot{\rho}_\chi + 3H(\rho_\chi + P_\chi) = n_\phi^{\rm eq} n_\psi \langle\sigma v \cdot E\rangle_{\psi\to\chi} - n_\phi^{\rm eq} n_\chi \langle\sigma v \cdot E\rangle_{\chi\to\psi}. \tag{4}$$

Here $n_{\phi,\psi}$ are the ϕ and ψ number densities respectively, with equilibrium values indicated with superscript "eq." Assuming χ maintains a Maxwell-Boltzmann distribution, the Boltzmann equations reduce to coupled partial differential equations for T_χ and n_χ as function of t (or T). The $3 \to 2$ cross section can be computed in a given model in terms of the parameters of the theory; at this stage we use a general parametrization at the mechanism level using dimensional analysis as [5]

$$\langle \sigma v^2 \rangle_{3\to 2} \equiv \frac{\alpha^3}{m_\chi^5}, \tag{5}$$

with α an effective coupling strength.

For the inelastic scattering process, the thermally averaged cross section and energy transfer terms are given by

$$n_\phi^{\rm eq} n_\chi \langle \sigma v \rangle_{\chi\to\psi} = \int d\Pi_\chi d\Pi_{\phi_1} d\Pi_\psi d\Pi_{\phi_2} f_\chi f_{\phi_1} (2\pi)^4 \delta^{(4)}(\Sigma p) \overline{|\mathcal{M}|}^2_{\chi\to\psi} \tag{6}$$

and

$$n_\phi^{\rm eq} n_\chi \langle \sigma v \cdot E \rangle_{\chi\to\psi} = \int d\Pi_\chi d\Pi_{\phi_1} d\Pi_\psi d\Pi_{\phi_2} E_\chi f_\chi f_{\phi_1} (2\pi)^4 \delta^{(4)}(\Sigma p) \overline{|\mathcal{M}|}^2_{\chi\to\psi}, \tag{7}$$

where E represents the energy transferred from the dark sector particle to the bath. Here $\overline{|\mathcal{M}|}^2_{\chi\to\psi}$ is the averaged matrix element squared corresponding to the $\chi\phi \to \psi\phi$ process, and f_i is the phase space distribution of $i = \chi, \phi$. The backreaction terms in the Boltzmann equations can be found via detailed balance.

The exact calculation of these thermally averaged cross sections and energy transfers can be performed in specific models. Assuming a constant matrix element at low DM velocity and taking the leading low temperature and small mass splitting limit, we can write a general form for the energy transfer terms,

$$\langle \sigma v \cdot E \rangle_{\psi\to\chi} \simeq \frac{\epsilon^2}{m_\chi}\left(1 + \frac{\Delta x}{2}\right), \qquad \epsilon^2 \equiv \frac{g_\psi g_\phi \overline{|\mathcal{M}|}^2_{\chi\to\psi}}{128\pi}, \tag{8}$$

where ϵ is a dimensionless parametrization coefficient, $\Delta = (m_\psi - m_\chi)/m_\chi$, $x = \frac{m_\chi}{T}$ and $g_{\chi,\psi}$ indicating the number of degrees of freedom in each species. Similarly, we can find the thermally averaged cross section,

$$\langle \sigma v \rangle_{\psi\to\chi} \simeq \frac{\epsilon^2}{m_\chi^2}\left(1 + \frac{\Delta x}{2}\right). \tag{9}$$

The backreaction forbidden channel is exponentially suppressed in comparison to the nonforbidden channel,

$$\langle \sigma v \cdot E \rangle_{\chi\to\psi} \propto e^{-\Delta x}, \qquad \langle \sigma v \rangle_{\chi\to\psi} \propto e^{-\Delta x}, \tag{10}$$

taking leading order in Δx.

Equations (9) and (10) offer a qualitative understanding of the properties of the energy transfer and cross sections. In the computations below, we include also next order terms. Further details are given in Appendix A.

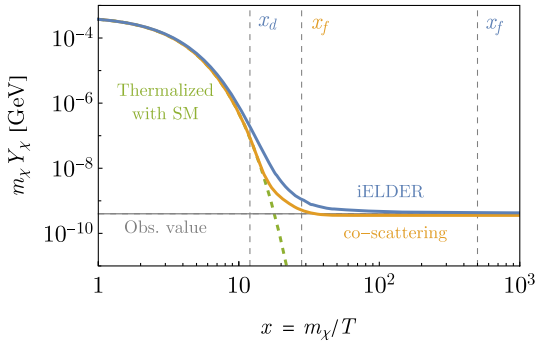


FIG. 2. Time evolution. DM yield times mass $m_\chi Y_\chi$ as a function of $x \equiv m_\chi/T$ with $m_\chi = 10$ MeV, $\Delta = 0.1$, $\epsilon = 2\times 10^{-8}$ (2.5×10^{-8}) and $\alpha = 5$ (0.5) for iELDER (coscattering) DM, reproducing the observed abundance. We indicate the x values corresponding to iELDER (blue) and coscattering (orange) decoupling and freeze out. At early times (small x), DM remains in thermal equilibrium with the SM bath due to the $\chi \leftrightarrow \psi$ inelastic scattering. In the iELDER regime, this process decouples first, separating the DM bath from the SM bath. The DM then cannibalizes until the $3 \to 2$ process freezes out. In contrast, in the coscattering regime, the $3 \to 2$ self-annihilations shuts off first, and DM freeze-out occurs when the inelastic scattering is no longer active.

We remark that the use of integrated Boltzmann equations implicitly assumes that χ particles are in kinetic equilibrium at late times. This assumption can be easily justified if we assume $2 \leftrightarrow 2$ self scattering with a coupling of order α. For reasonably large values, of order $\alpha \gtrsim 10^{-3}$, self-scattering will be active during and after freeze out, ensuring kinetic equilibrium throughout the process.

In what follows, we solve the coupled Boltzmann equations (3) and (4) numerically to obtain the time evolution and parameter space of this DM scenario. Figure 2 illustrates the time evolution of the DM number density in the iELDER and coscattering regimes for DM mass $m_\chi = 10$ MeV and mass splitting $\Delta = 0.1$ for fixed values of ϵ and α couplings that produce the observed DM relic abundance. At early times (small x), χ is thermalized with the bath, and so its yield $Y_\chi = n_\chi/s$ follows a Boltzmann distribution and drops exponentially at nonrelativistic temperatures. In the iELDER regime (blue curve), the inelastic scattering process decouples first, at $x_d \sim \mathcal{O}(10)$, χ detaches from the SM bath and cannibalizes through $3 \to 2$ self-annihilations, resulting in a yield that decreases slowly. Later, at $x_f \sim \mathcal{O}(100)$, when the self-annihilations also shut off, the DM abundance freezes out to its observed value. In contrast, in the coscattering regime (orange curve), the $3 \to 2$ self-annihilations freeze out first. The DM abundance is then determined by the freeze out of the inelastic coscattering process, at $x_f \sim \mathcal{O}(10'\,\mathrm{s})$. (Analytical approximations for x_f and x_d in the iELDER case are provided in Appendix B.)

Figure 3 shows the $\epsilon - \alpha$ phase space for a range of DM masses and mass splittings. As predicted, we find two

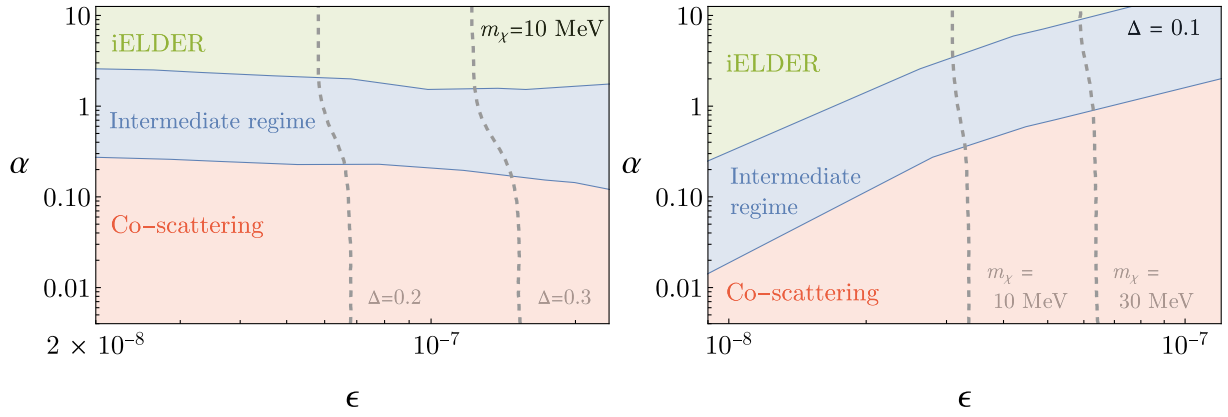


FIG. 3. Phases of the setup. Partition of the $\epsilon - \alpha$ parameter space [defined via Eqs. (5) and (8)] to the distinct production mechanisms of coscattering (red) and iELDER (green), with an intermediate regime (blue) marking the smooth transition between the phases. Left: the three phases for a fixed DM mass of $m_\chi = 10$ MeV and varying mass splittings. We show representative curves for $\Delta = 0.2, 0.3$. Right: the same phases for fixed mass splitting $\Delta = 0.1$ and varying DM masses above an MeV. We show representative curves of $m_\chi = 10, 30$ MeV.

distinct regimes that reproduce the DM relic abundance, with a continuous transition between them. We show the partition of the phase space into the different phases—the left panel for fixed DM mass and varying the mass splitting, and the right panel reversed. We also show representative curves for fixed values of Δ (left) and m_χ (right), delineating how the couplings transition. Along the upper part of each curve, corresponding to large values of α, the inelastic scattering process decouples first, creating an iELDER phase. As one flows along the curves to lower values of α, the $3 \to 2$ process decouples first, and the system enters the coscattering regime. The value of ϵ only slightly varies between the two phases, because in both cases it is the decoupling of same inelastic scattering process that controls the abundance. For iELDER the abundance is determined by the kinetic decoupling of the inelastic scattering, and for coscattering the abundance is determined by the chemical decoupling of the same process.

III. TOY Z_3 MODEL

We now present an effective model that realizes the phases presented in Sec. II. Consider a DM candidate χ that is a complex scalar charged under an unbroken Z_3 symmetry. The effective Lagrangian for such a model is given by

$$\mathcal{L} \supset \frac{R}{3!} m_\chi \chi^3 + \text{H.c.} \tag{11}$$

There is, in principle, also a $\lambda_\chi |\chi|^4$ term which will contribute to the full $3 \to 2$ process, however for simplicity we set $\lambda_\chi = 0$ (see also Ref. [12]). This results in a thermally averaged cross section

$$\langle \sigma v^2 \rangle_{3\to 2} \simeq 10^{-4} \frac{R^6}{m_\chi^5}, \tag{12}$$

that relates R with α defined in Eq. (5). The Lagrangian will also include a 4-point interaction term, involving the interaction of the DM χ with a heavier scalar ψ of mass $m_\psi = m_\chi(1 + \Delta)$ and a pair of photons or fermions. We consider two possibilities,

$$\mathcal{L}_\gamma \supset \frac{1}{\Lambda_\gamma^2} \chi^\dagger \psi F_{\mu\nu} F^{\mu\nu} + \text{H.c.}, \tag{13}$$

and

$$\mathcal{L}_e \supset \frac{m_e}{\Lambda_e^2} \chi^\dagger \psi \bar{e} e + \text{H.c.}, \tag{14}$$

with e the electron; the generalization to other fermions is straightforward.

This Z_3 model yields Boltzmann equations of similar form to Eqs. (3) and (4), with $\phi = \gamma$ or e. If coupling to photons, the dimensionless coefficient ϵ^2 related to the rate of the inelastic scattering as defined in Eqs. (8) and (9) is

$$\epsilon_\gamma^2 \simeq \frac{m_\chi^4}{32\pi\Lambda_\gamma^4}, \tag{15}$$

and if coupling to electrons,

$$\epsilon_e^2 \simeq \frac{3 m_e^4}{16\pi\Lambda_e^4}. \tag{16}$$

One can now numerically solve the Boltzmann equations for the model. The $\alpha - \epsilon_\phi$ coupling phase space (with ϕ either photons or electrons) is similar to that obtained for

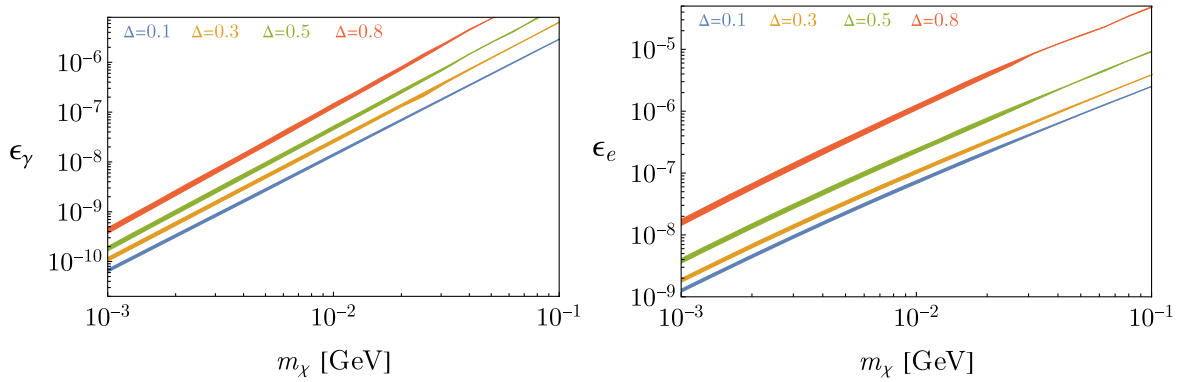


FIG. 4. $\boldsymbol{Z_3}$ model. The coupling to photons ϵ_γ (left) and electrons ϵ_e (right) as a function of m_χ in the Z_3 toy model across all DM phases, derived from the numerical solution to the Boltzmann equations, for DM self-couplings $R \lesssim 4\pi$ and fixed mass splittings Δ.

the general case in Fig. 3. In Fig. 4 we show the values of ϵ_γ (left panel) and ϵ_e (right panel) as a function of m_χ, for various fixed mass splittings, that produce the observed DM relic abundance for perturbative self-couplings R across all phases. The allowed couplings are given by colored regions that appear as a curve with varying thickness. The thickness of the colored region grows for larger mass splittings Δ, as a result of a larger intermediate phase between the coscattering and iEDLER regimes, namely a larger difference between the solutions in these two phases. For $m_\chi \gtrsim 40$ MeV, the allowed variation in the values of the inelastic couplings ϵ_γ and ϵ_e is restricted because the iELDER phase cannot be found for perturbative self-couplings $R \lesssim 4\pi$.

We do not discuss existing constraints or future projections of this toy model. We move to a more realistic and phenomenologically relevant realization of the iELDER phase in QCD-like theories, next.

IV. QCD-LIKE PION MODEL

Having described the iELDER mechanism and demonstrating it in a toy theory, we now move to presenting a more realistic model, under the assumptions of case (ii). We consider QCD-like theories admitting $3 \to 2$ self-annihilations, which have been considered in the past as the SIMPlest realization of SIMP DM [6,20]. In these theories of dynamical chiral symmetry breaking, the pseudo-Nambu Goldstone bosons of the theory—which we will collectively call pions—can play the role of DM, with the Wess-Zumino-Witten (WZW) term [21–23] generating the $3 \to 2$ annihilation process.

A. SIMPlest setup

Consider the SIMPlest scenario with an $SU(2)_c$ gauge symmetry and 4 Weyl fermions q_i. The kinetic terms preserve an $SU(4)$ flavor symmetry,

$$\mathcal{L}_{\rm kin} = i\bar{q}_i \not{D} q_i. \tag{17}$$

This model leads to chiral symmetry breaking with the order parameter

$$\langle q_i \bar{q}_j \rangle = \mu^3 J_{ij}, \tag{18}$$

where μ is a mass-dimension-one parameter and $J = i\sigma_2 \otimes \mathbb{1}_2$ is a 4×4 anti-symmetric matrix that preserves the flavor subgroup $Sp(4) \subset SU(4)$ [23–26]. There are $N_\pi = 5$ (Nambu Goldstone boson) pion fields π^a, $a = 1, \ldots 5$, which will play the role of DM. We use the parametrization [6]

$$\Sigma = \exp(2i\pi/f_\pi)J \tag{19}$$

for the coset space $SU(4)/Sp(4)$, with

$$\pi = \begin{pmatrix} \frac{\pi_3}{\sqrt{2}} & \frac{\pi_1 - i\pi_2}{\sqrt{2}} & 0 & \frac{\pi_4 - i\pi_5}{\sqrt{2}} \\ \frac{\pi_1 + i\pi_2}{\sqrt{2}} & -\frac{\pi_3}{\sqrt{2}} & -\frac{\pi_4 + i\pi_5}{\sqrt{2}} & 0 \\ 0 & -\frac{\pi_4 + i\pi_5}{\sqrt{2}} & \frac{\pi_3}{\sqrt{2}} & \frac{\pi_1 + i\pi_2}{\sqrt{2}} \\ \frac{\pi_4 + i\pi_5}{\sqrt{2}} & 0 & \frac{\pi_1 - i\pi_2}{\sqrt{2}} & -\frac{\pi_3}{\sqrt{2}} \end{pmatrix}, \tag{20}$$

and f_π the pion decay constant. The 5-point interactions, yielding the $3 \to 2$ self annihilations, are generated by the WZW term. Under our parametrizations, to leading order in pion fields, we have

$$\mathcal{L}_{\rm WZW} = \frac{4}{15\pi^2 f_\pi^5} \epsilon^{\mu\nu\rho\sigma} {\rm Tr}[\pi \partial_\mu \pi \partial_\nu \pi \partial_\rho \pi \partial_\sigma \pi]. \tag{21}$$

We take a $U(1)_D$ subgroup of the flavor symmetry to be gauged, corresponding to the generator $Q_D = {\rm diag}\{1, 1, -1, -1\}$, which breaks $SU(4) \to SU(2) \times U(1)_D$. The $U(1)_D$ is spontaneously broken by the VEV of a scalar field ϕ that carries charge -2. This introduces Yukawa couplings that induce symmetry breaking masses,

$$\mathcal{L}_\phi \supset \lambda\phi\epsilon_{ij}Q_iQ_j + \bar{\lambda}\phi^*\epsilon_{ij}\bar{Q}_i\bar{Q}_j + \text{H.c.} \equiv K_{ij}q_iq_j + \text{H.c.} \tag{22}$$

where $Q = (q_1, q_2)$, $\bar{Q} = (q_3, q_4)$, and

$$K = \begin{pmatrix} 0 & m_D & 0 & 0 \\ -m_D & 0 & 0 & 0 \\ 0 & 0 & 0 & \bar{m}_D \\ 0 & 0 & -\bar{m}_D & 0 \end{pmatrix}, \tag{23}$$

with Dirac masses $m_D = \lambda\langle\phi\rangle$, $\bar{m}_D = \bar{\lambda}\langle\phi\rangle^*$ [27]. The total quark mass term is given by

$$\mathcal{L}_{\text{mass}} = -\frac{1}{2}M^{ij}q_iq_j + \text{H.c.}, \tag{24}$$

where

$$M = m_Q J - 2K \tag{25}$$

and $m_Q J$ is the $Sp(4)$-preserving mass contribution. For simplicity, we will consider the case of $m_D = \bar{m}_D$, which assumes an additional charge symmetry $Q \leftrightarrow \bar{Q}$. (For a full study of symmetries of the low energy mesonic spectrum of SIMPlest scenario, see Ref. [27].)

The pions acquire mass,

$$\begin{aligned}\mathcal{L}_{\text{eff}} &\supset -\frac{1}{2}\mu^3\text{Tr}M\Sigma + \text{H.c.} \\ &= -\frac{m_\pi^2}{4}\text{Tr}\pi^2 + \frac{m_\pi^2}{12f_\pi^2}\text{Tr}\pi^4 + \mathcal{O}\left(\frac{\pi^6}{f_\pi^4}\right),\end{aligned} \tag{26}$$

where $m_\pi^2 \equiv 8(m_Q\mu^3)/f_\pi^2$ with the $Sp(4)$-breaking contribution K canceling in the Hermitian conjugate. The symmetry breaking in masses will manifest in the second order term,

$$\begin{aligned}\Delta\mathcal{L}_{\text{eff}} &= \eta f_\pi^2\text{Tr}M\Sigma M\Sigma + \text{H.c.} \\ &= -\frac{\eta f_\pi^4 m_\pi^4}{4\mu^6}\text{Tr}\pi^2 - 64\eta m_D^2\pi_4^2 + \frac{1024\eta m_D^2}{3f_\pi^2}\pi_4^2\text{Tr}\pi^2 \\ &\quad + \frac{8\eta f_\pi^2 m_\pi^4}{3\mu^6}\text{Tr}\pi^4 + \mathcal{O}\left(\frac{\pi^6}{f_\pi^4}\right),\end{aligned} \tag{27}$$

where η is a dimensionless coefficient. This term introduces a correction to the pion mass, and a mass splitting between π_4 and the other pions. The resulting pion masses are

$$m_{1,2,3,5}^2 = \tilde{m}_\pi^2, \qquad m_4^2 = \tilde{m}_\pi^2(1+\Delta), \qquad \Delta = \frac{256\eta m_D^2}{\tilde{m}_\pi^2}, \tag{28}$$

where $\tilde{m}_\pi^2 = m_\pi^2\left(1 + 64\eta\frac{m_Q^2}{m_\pi^2}\right)$. In addition, terms introduced in Eqs. (26) and (27) generate 4-point pion self-scattering.

The kinetic term also generates terms inducing pion self-scattering, in addition to a 3-point interaction involving π_4, π_5 and the dark gauge field $\mathcal{A}_\mu$ of the gauged $U(1)_D$,

$$\begin{aligned}\mathcal{L}_{\text{kin}} &= \frac{f_\pi^2}{16}D_\mu\Sigma D^\mu\Sigma^\dagger \\ &= \frac{1}{4}\text{Tr}\partial_\mu\pi\partial^\mu\pi - \frac{1}{6f_\pi^2}\text{Tr}(\pi^2\partial_\mu\pi\partial^\mu\pi - \pi\partial_\mu\pi\pi\partial^\mu\pi) \\ &\quad + \frac{e_D}{4}\mathcal{A}^\mu(\pi_5\partial_\mu\pi_4 - \pi_4\partial_\mu\pi_5) + \mathcal{O}\left(e_D^2, \frac{\pi^6}{f_\pi^4}\right).\end{aligned} \tag{29}$$

$\mathcal{A}_\mu$ has kinetic mixing with the $U(1)_Y$ gauge field B_μ [20,28,29],

$$\mathcal{L}_{\mathcal{A}} = -\frac{1}{4}\mathcal{A}_{\mu\nu}\mathcal{A}^{\mu\nu} - \frac{\sin\chi}{2}B_{\mu\nu}\mathcal{A}^{\mu\nu} + \frac{1}{2}m_A^2\mathcal{A}_\mu\mathcal{A}^\mu, \tag{30}$$

with $\mathcal{A}_{\mu\nu}$ and $B_{\mu\nu}$ the respective field strengths. When electroweak symmetry breaking occurs, $\mathcal{A}_\mu$ becomes a mixture of the Z-boson and the dark photon V,

$$V^\mu = -\frac{\sin\zeta}{\cos\chi}Z^\mu + \frac{\cos\zeta}{\cos\chi}\mathcal{A}^\mu, \tag{31}$$

where

$$\tan 2\zeta = \frac{m_Z^2\sin\theta_W\sin 2\chi}{m_A^2 - m_Z^2(\cos^2\chi - \sin^2\theta_W\sin^2\chi)}, \tag{32}$$

and θ_W the weak mixing angle. This generates a $\pi_4 f \leftrightarrow \pi_5 f$ inelastic scattering process and a $\pi_4\pi_5 \to f\bar{f}$ annihilation process, both mediated by a dark photon V_μ, where f is a SM fermion. For light DM, the leading processes involve abundant electrons; we thus consider this leading contribution of $f = e$ in what follows.

B. SIMPlest boltzmann equations

The Boltzmann equations governing the pion system include number changing processes: the $3 \to 2$ pion self-annihilation generated by the WZW term and the $\pi_4\pi_5 \to e^+e^-$ coannihilation that originates from the kinetic mixing with the SM. The inelastic scattering process ($\pi_4 e^\pm \to \pi_5 e^\pm$) generated by the mixing does not alter the total pion number. Two-to-two DM self-annihilations will be the last processes to decouple. As a result, all the pions will be in chemical equilibrium, and the heavier pion π_4 will eventually annihilate to the lighter pions. Thus, the number density Boltzmann equation for the pions will be

$$\dot{n}_\pi + 3Hn_\pi = -\langle\sigma v\rangle_{\rm ann}^{\rm eff}(n_\pi^2 - (n_\pi^{\rm eq})^2) - \langle\sigma v^2\rangle_{3\to2}((n_\pi)^3 - n_\pi^{\rm eq}(n_\pi)^2), \quad (33)$$

where $n_\pi^{(\rm eq)} = \sum_{i=1}^5 n_{\pi_i}^{(\rm eq)}$. The $3\to2$ thermally averaged cross section up to leading order in Δ is

$$\langle\sigma v^2\rangle_{3\to2} \simeq \langle\sigma v^2\rangle_{3\to2}^{\Delta=0}\left(1+\frac{14}{125}\Delta\right), \quad (34)$$

where $\langle\sigma v^2\rangle_{3\to2}^{\Delta=0}$ is the cross section for the nonbroken case calculated in Ref. [12], arising from the WZW term,

$$\langle\sigma v^2\rangle_{3\to2}^{\Delta=0} = \frac{24\sqrt{5}\tilde{m}_\pi^5}{5\pi^5 f_\pi^{10} x_\pi^2}. \quad (35)$$

The effective coannihilation process between π_4 and π_5 (up to leading order in Δ) is described by

$$\langle\sigma v\rangle_{\rm ann}^{\rm eff} = \frac{n_{\pi_4}^{\rm eq} n_{\pi_5}^{\rm eq}}{(n_\pi^{\rm eq})^2}\langle\sigma v\rangle_{\rm ann} \simeq e^{-\Delta x_\pi}\frac{\alpha_D\alpha_{\rm EM}\epsilon_\gamma^2\tilde{m}_\pi^2}{x_\pi m_V^4}. \quad (36)$$

Here $\langle\sigma v\rangle_{\rm ann}$ is the $\pi_4\pi_5 \to e^+e^-$ thermally averaged cross section, $x_\pi = \frac{\tilde{m}_\pi}{T_\pi}$ with T_π the temperature of the pions, m_V the mass of the dark photon, $\alpha_{\rm EM}$ (α_D) is the (dark) fine structure constant, and we define

$$\epsilon_\gamma \equiv -\cos\theta_W\cos\zeta\tan\chi \quad (37)$$

as a dimensionless coefficient related to the mixing angle.

To evaluate the pion temperature we also need to solve the energy density Boltzmann equation,

$$\dot{\rho}_\pi + 3H(\rho_\pi + P_\pi) = n_e^{\rm eq} n_{\pi_4}\langle\sigma v\cdot\delta E\rangle_{4\to5} - n_e^{\rm eq} n_{\pi_5}\langle\sigma v\cdot\delta E\rangle_{5\to4}, \quad (38)$$

where $\rho_\pi = \sum_{i=1}^5\rho_i$, $P_\pi = \sum_{i=1}^5 P_i$ and $\langle\sigma v\cdot\delta E\rangle_{i\to j}$ is the energy transfer rate generated by the $\pi_4 e^\pm \to \pi_5 e^\pm$ inelastic scattering, with $i, j = 4, 5$, which can be calculated at leading order in small Δ, large $x = \frac{\tilde{m}_\pi}{T}$ and $x_\pi \sim x$,

$$\langle\sigma v\cdot\delta E\rangle_{4\to5} \simeq \frac{3\tilde{m}_\pi m_e^2\alpha_D\alpha_{\rm EM}\epsilon_\gamma^2}{4\pi m_V^4}\frac{x-x_\pi}{x}\left(1+\frac{\Delta x^3}{4}\right), \quad (39)$$

and

$$\langle\sigma v\cdot\delta E\rangle_{5\to4} \simeq e^{-\Delta x}\langle\sigma v\cdot\delta E\rangle_{4\to5}. \quad (40)$$

C. SIMPlest results

Figure 5 shows our numerical solution to the Boltzmann equations for the pion model, Eqs. (33) and (38), where we obtain the $\tilde{m}_\pi/f_\pi$ and ϵ_γ relation that produces the observed DM abundance, for various DM masses and mass splittings. In the left panel, we fix the mass splittings and vary the DM mass, and in the right panel we fix the DM mass and vary the mass splitting. We find three distinct regimes depending on the decoupling order of the $3\to2$ self-annihilations, the inelastic scattering and the $\pi_4\pi_5$ annihilations (see also depiction of case (ii) in Fig. 1). $\pi_4\pi_5$ annihilations always decouple before the inelastic scattering process. At small values of $\tilde{m}_\pi/f_\pi$, the $3\to2$ self-annihilations shut off before $\pi_4\pi_5$ annihilations, resulting in a coannihilation phase. The relic abundance is then controlled by the annihilation process whose rate depends on the coupling to the bath ϵ_γ and is insensitive to the ratio

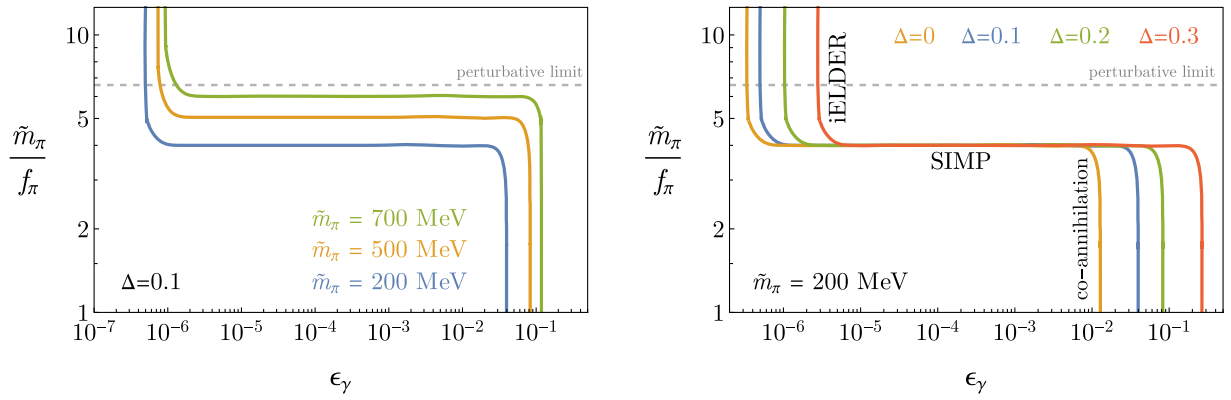


FIG. 5. SIMPlest pion model phase diagram. $\tilde{m}_\pi/f_\pi$ as the function of ϵ_γ derived from the numerical solution to the Boltzmann Equations for various DM masses $\tilde{m}_\chi$ and mass splittings Δ, with $m_V = 3\tilde{m}_\pi$ and $\alpha_D = 0.1$. Three regimes of the phase space emerge. In all cases, $\pi_4\pi_5$ annihilations decouple before the inelastic scattering process. At small values of $\tilde{m}_\pi/f_\pi$, the $3\to2$ self-annihilations shut off before $\pi_4\pi_5$ annihilations, resulting in a coannihilation phase where the DM abundance is determined by ϵ_γ. As one flows to larger values of $\tilde{m}_\pi/f_\pi$, $3\to2$ self-annihilations decouple after $\pi_4\pi_5$ annihilations but before the inelastic scattering process shuts off, leading to a SIMP regime, where the DM abundance is determined by $\tilde{m}_\pi/f_\pi$. Finally, for even larger values of $\tilde{m}_\pi/f_\pi$, inelastic scattering decouples before $3\to2$ self-annihilations, and an iELDER phase emerges, with the DM abundance set by ϵ_γ.

$\tilde{m}_\pi/f_\pi$. At larger values of $\tilde{m}_\pi/f_\pi$, $3 \to 2$ self-annihilations decouple after $\pi_4\pi_5$ annihilations but before the inelastic scattering process shuts off, leading to a SIMP regime. Here the DM relic abundance is set by $\tilde{m}_\pi/f_\pi$ and is insensitive to ϵ_γ. Finally, for even larger values of $\tilde{m}_\pi/f_\pi$, inelastic scattering decouples before $3 \to 2$ self-annihilations, and an iELDER phase emerges, where ϵ_γ again determines the DM abundance. We note that typical values for x_d, x_f remain of similar size to the model-independent approach detailed above, where $x_d \sim \mathcal{O}(10)$ and $x_f \sim \mathcal{O}(100)$ for the iELDER scenario, and $x_f \sim \mathcal{O}(10's)$ in the SIMP and coannihilation scenarios.

For a fixed value of Δ, as we increase the value of the DM mass we shift the phase space accordingly. In the SIMP regime, higher masses correspond to higher values of $\tilde{m}_\pi/f_\pi$, and in the other two regimes of coannihilation and iELDER, to higher values of ϵ_γ. At fixed DM mass, a change in the mass splitting results in a very small change of the SIMP phase solution, with a larger impact on the couplings in the iEDLER and coannihilation phases. The reason is that the $3 \to 2$ self-annihilation cross section is weakly dependent on Δ [as in Eq. (34)], whereas the annihilation and inelastic scattering cross sections have an exponential dependence on Δ [as in Eqs. (36) and (40)], yielding greater sensitivity to Δ.

Although four–pion interactions do not fix the relic abundance, they will constrain the pion mass range. Eqs. (26), (27), and (29) generate elastic $2 \to 2$ self-scatterings among all the pion states. After freeze-out, the heavy pions (π_4) will efficiently down-scatter into lighter species, so only the four light pions contribute to the dark matter self-scattering cross section today, σ_{scatter}. Astrophysical observations such as the Bullet Cluster collision and the shapes of galactic halos [30–36] constrain

$$\frac{\sigma_{\text{scatter}}}{m_{\text{DM}}} \lesssim 1 \text{ cm}^2/\text{g}. \tag{41}$$

Following [6], the self-scattering cross section is

$$\sigma_{\text{scatter}} = \frac{35\tilde{m}_\pi^2}{192\pi f_\pi^4}, \tag{42}$$

and thus Eq. (41) translates into an upper limit on the ratio $\tilde{m}_\pi/f_\pi$ for any given mass.

In addition, to this astrophysical constraint, we also consider the chiral perturbation theory requirement of $\tilde{m}_\pi/f_\pi \lesssim 2\pi$. The combined results are shown in Fig. 6. The shaded band at the top, outlined by the dashed gray curve, indicates where perturbativity is lost, while the shaded region outlined by the dot-dashed gray curve indicates where the self-interaction constraint of Eq. (41) is not met. The different mechanisms setting the relic abundance in this parameter space—coannihilation, SIMP, and iELDER—are indicated by the three colored regions.

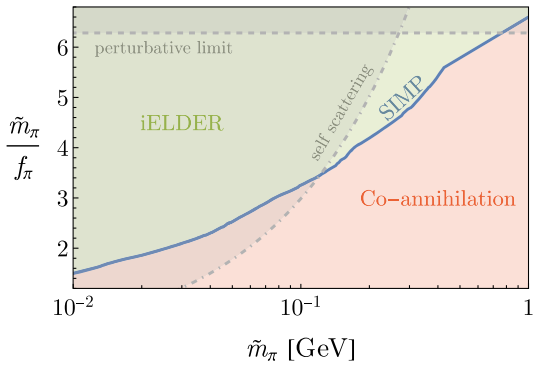


FIG. 6. Allowed parameter space in the SIMPlest pion model. The ratio $\tilde{m}_\pi/f_\pi$ as a function of the dark pion mass $\tilde{m}_\pi$, for $m_V = 3\tilde{m}_\pi$, $\Delta = 0.1$, $\alpha_D = 0.1$ and a range of ϵ_γ. Different colors indicate the mechanism that sets the DM relic abundance across the parameter space: coannihilation (shaded red), SIMP (blue curve), and iELDER (shaded green). The upper shaded gray region indicates the perturbativity limit of $\tilde{m}_\pi/f_\pi \lesssim 2\pi$, while the lower shaded gray region is in tension with the self-scattering constraint of Eq. (41).

We learn that the viable iELDER parameter space in this pion theory is constrained to the mass range

$$130 \text{ MeV} \lesssim \tilde{m}_\pi \lesssim 800 \text{ MeV}, \tag{43}$$

where both self-interaction bounds and perturbativity are satisfied. For larger values of m_π/f_π, lattice calculations show that the corrections to the self-scattering are large, but are expected to lower the cross section relative to the leading order result [37]. Due to the large uncertainty in the self-scattering bound and the large lattice corrections, we consider Eq. (41) as a naive approximate constraint on Eq. (42). (Note that in light of the uncertainties, Eq. (42) neglects the second order contributions to the self-interaction rate that appear in Eq. (27).)

Figure 7 shows the experimental prospects for the SIMPlest pion model presented here in its various phases (see also Ref. [38]). The parameter space is constrained by data from dark photon decays at beam-dump experiments such as NuCal and CHARM at CERN [39], LSND [40], missing energy searches at *BABAR* [41], and down- or up-scattering in E137 at SLAC, LSND and MiniBooNE [42]. Future experiments will extend the reach into new regions of parameter space via dark photon decays in beam-dump experiments at Fermilab such as SeaQuest [43], PIP2-BD [44] and the short baseline experiments (SBND, MicroBooNE and ICARUS) [45], in addition to the JNSS^2 beam dump neutrino experiment at J-PARK [40]. Other future prospects include decays of the dark photon at particle colliders such as Belle-II at SuperKEKB [46], and the FASER detector at the LHC [41]. Figure 7 shows the existing constraints (shaded colored regions) and future projections (dashed colored curves) on our parameter space for fixed

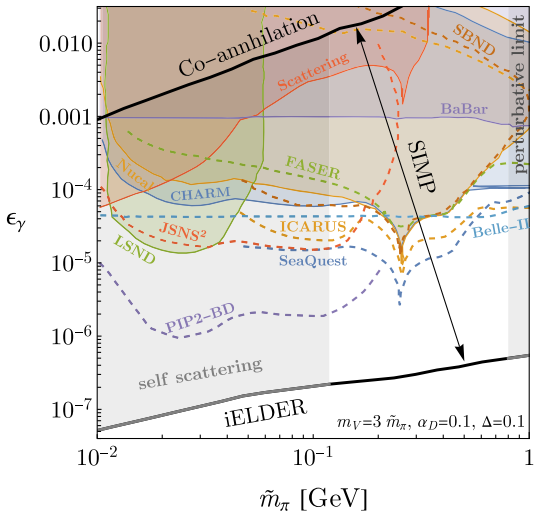


FIG. 7. SIMPlest pion model phenomenology. Existing constraints (shaded regions) and future projections (dashed curves) on ϵ_γ and $\tilde{m}_\pi$ for the pion model, with $m_V = 3\tilde{m}_\pi, \Delta = 0.1$ and $\alpha_D = 0.1$. Solid black curves indicate the numerical solution to the Boltzmann equations producing the observed DM relic abundance for the coannihilation and iELDER regimes (upper and lower curves, respectively); the region spanned between these two curves corresponds to the SIMP regime. The parameter space is constrained by data from NuCal and CHARM [39], LSND [40,42], *BABAR* [41], E137 and MiniBooNE [42]. Projections are shown for future experiments, including SeaQuest [43], PIP2-BD [44], short baseline experiments (SBND, MicroBooNE and ICARUS) [45], FASER [41], JNSS^2 [40] and Belle-II [46]. Gray shaded regions are in tension with self-scattering constraints (left) and the perturbativity limit (right).

values of m_V, α_D and Δ, and a range of DM masses and kinetic mixings ϵ_γ. The upper and lower solid black curves indicate where the numerical solution to the Boltzmann equations produces the observed relic abundance in the coannihilation and iELDER scenarios, respectively, with the area between the black lines corresponding to the SIMP scenario. We indicate in shaded gray regions that are in tension with naive limits from self-scattering and perturbativity.

While the coannihilation regime is in general excluded by current experimental measurements for the considered benchmark parameter values, the SIMP regime is partially probed and set to be further covered in upcoming experiments, with the iELDER phase laying just beyond the reach of planned future experiments.

V. SUMMARY

In this work, we introduced iELDER as a new framework for thermal DM production. In this scenario, the DM relic abundance is set by an *inelastic* scattering process—the decoupling of DM–bath scattering—while $3 \to 2$ self-annihilations remain active in the dark sector. Compared to coscattering or elastically decoupling relics, iELDER DM is distinct in its thermal evolution and hierarchy of decoupling processes. iELDER predicts DM in the MeV to GeV mass range along with heavier dark particles not too far in mass, with large $3 \to 2$ self-annihilations and weak inelastic interactions with bath particles.

We demonstrated that iELDER DM emerges in scenarios where the DM particle scatters off another particle whose chemical potential remains zero during freeze-out, due to interactions either with the SM bath or with the dark sector. In the first case, we solved the coupled Boltzmann equations for the DM number and energy densities in the presence of inelastic scattering and $3 \to 2$ self-annihilations, using a parametrization that is agnostic to the microscopic origin of such interactions. This setup admits a phase diagram partitioned into an iELDER regime and a coscattering one, with an intermediate transition between the two phases. A toy Z_3 theory with effective couplings of the DM to either photons or electrons provided a simplified benchmark model that realized these phases. We further presented well-motivated QCD-like theories that realize the second case, utilizing a variation of the dark pion models originally formulated to produce SIMP DM. We derived experimental constraints and future projections on this QCD-like theory, leading to interesting phenomenology that can be probed in the near future.

Incorporating DM inelastic scattering alongside DM self-annihilations offers a rich extension to the thermal DM landscape, with phenomenological implications. Further model-building efforts to construct theories that realize such a scenario would further our understanding of how to constrain or detect iEDLER dark matter.

ACKNOWLEDGMENTS

We thank Hitoshi Murayama for useful discussions. The work of Y. H. is supported by the Israel Science Foundation (Grant No. 1818/22), by the Binational Science Foundation (Grant No. 2022287) and by an ERC STG grant ("Light-Dark," Grant No. 101040019). E. K. is supported by NSF-BSF (Grants No. 2022713 and No. 2023711) and by the US-Israeli Binational Science Foundation (Grant No. 2020220). B. V. acknowledges support by the Israel Science Foundation (Grant No. 1818/22). This project has received funding from the European Research Council (ERC) under the European Union's Horizon Europe research and innovation programme (grant agreement No. 101040019).

Views and opinions expressed are however those of the author(s) only and do not necessarily reflect those of the European Union. The European Union cannot be held responsible for them.

DATA AVAILABILITY

The data that support the findings of this article are not publicly available upon publication because it is not technically feasible and/or the cost of preparing, depositing,

and hosting the data would be prohibitive within the terms of this research project. The data are available from the authors upon reasonable request.

APPENDIX A: ENERGY TRANSFER CALCULATION

In this appendix, we lay out the full calculation of the iELDER energy transfer that we use for our results. We will begin with calculating the energy transfer of the forbidden reaction $\langle\sigma v\cdot E\rangle_{\chi\to\psi}$ depending on both χ's temperature T_2 and the bath's temperature T, under the assumptions of case (i). Then we will obtain the forward reaction energy transfer $\langle\sigma v\cdot E\rangle_{\psi\to\chi}$ via detailed balance, taking $T_2\to T$.

To this end, we need to compute the following integral

$$n_\phi^{\rm eq} n_\chi\langle\sigma v\cdot E\rangle_{\chi\to\psi}=\int d\Pi_\chi d\Pi_{\phi_1} d\Pi_\psi d\Pi_{\phi_2} E_\chi f_\chi f_{\phi_1}(2\pi)^4\delta^{(4)}(p_1+p_2-k_1-k_2)\overline{|\mathcal{M}|}^2_{\chi\to\psi}. \tag{A1}$$

Here $\overline{|\mathcal{M}|}^2_{\chi\to\psi}$ is the squared matrix element averaged over initial and final states corresponding to the $\chi\phi\to\psi\phi$ process, $d\Pi_i=\frac{g_i d^3p_i}{(2\pi)^3 2E_i}$, p_1 and p_2 are the ingoing momentum of χ and ϕ_1 respectively, k_1 and k_2 the outgoing momentum of ψ and ϕ_2, and we assume the simple form for the phase space distribution $f_i=e^{-\frac{E_i}{T_i}}$. We use

$$\begin{aligned}&\int d\Pi_i d\Pi_j(2\pi)^4\delta^{(4)}(p_1'+p_2'-k_1'-k_2')\\&=g_i g_j\frac{\beta(s)}{8\pi}\int_{\cos\theta=-1}^{\cos\theta=1}\frac{d\cos\theta}{2}\frac{d\phi}{2\pi},\end{aligned} \tag{A2}$$

and so we find

$$\begin{aligned}n_\phi^{\rm eq} n_\chi\langle\sigma v\cdot E\rangle_{\chi\to\psi}=&\int d\Pi_\chi d\Pi_{\phi_1} E_\chi f_\chi f_{\phi_1} g_\psi g_{\phi_2}\frac{\beta(s)}{8\pi}\\&\Theta(s-m_\psi^2)\int_{\cos\theta=-1}^{\cos\theta=1}\frac{d\cos\theta}{2}\frac{d\phi}{2\pi}\overline{|\mathcal{M}|}^2_{\chi\to\psi},\end{aligned} \tag{A3}$$

where Θ stands for the Heaviside step function. Here s is the Mandelstam variable $s=(p_1+p_2)^2$,

$$\beta(s)=\sqrt{1-\frac{2m_\psi^2}{s}+\frac{m_\psi^4}{s^2}}=\left(1-\frac{m_\psi^2}{s}\right), \tag{A4}$$

and (θ,ϕ) are the angles in the center of mass frame. The matrix element for $2\to2$ scattering does not depend on ϕ, so the integration over it is trivial,

$$\begin{aligned}n_\phi^{\rm eq} n_\chi\langle\sigma v\cdot E\rangle_{\chi\to\psi}=&\frac{g_\chi g_{\phi_1} g_\psi g_{\phi_2}}{8(2\pi)^5}\int\frac{p_1^2p_2^2dp_1dp_2d\cos\theta_{p_1p_2}}{E_\chi E_{\phi_1}}\\&\times E_\chi f_\chi f_{\phi_1}\beta(s)\Theta(s-m_\psi^2)\\&\times\int_{\cos\theta=-1}^{\cos\theta=1}\frac{d\cos\theta}{2}\overline{|\mathcal{M}|}^2_{\chi\to\psi},\end{aligned} \tag{A5}$$

where $\theta_{p_1p_2}$ is the angle between p_1 and p_2. We assume a form $\overline{|\mathcal{M}|}^2_{\chi\to\psi}=c_{nl}s^n\cos^l\theta$ where $n,l\in\mathbb{N}$ and c_{nl} are real coefficients. We can solve the integral over $\cos\theta$, and by changing variables from $\cos\theta_{p_1p_2}$ to s using the relation

$$\begin{aligned}s&=\left(\sqrt{m_\chi^2+p_1^2}+p_2\right)^2-\left(\sqrt{p_1^2+p_2^2+2p_1p_2\cos\theta_{p_1p_2}}\right)^2\\&=\left(\sqrt{m_\chi^2+p_1^2}+p_2\right)^2-(p_1^2+p_2^2+2p_1p_2\cos\theta_{p_1p_2}).\end{aligned} \tag{A6}$$

Altogether the integral takes a simpler form,

$$\begin{aligned}n_\phi^{\rm eq} n_\chi\langle\sigma v\cdot E\rangle_{\chi\to\psi}=&\frac{g_\chi g_\phi g_\psi g_\phi}{16(2\pi)^5}\frac{c_{nl}}{l+1}\int\frac{p_1^2p_2^2dp_1dp_2}{E_\chi E_{\phi_1}}\frac{E_\chi f_\chi f_{\psi_1}}{2p_1p_2}\\&\times\int_{s_{\rm min}}^{s_{\rm max}}(s^n-m_\psi^2s^{n-1})\Theta(s-m_\psi^2)ds,\end{aligned} \tag{A7}$$

where the limits of integration are

$$\begin{aligned}s_{\rm min}&=\left(\sqrt{m_\chi^2+p_1^2}+\sqrt{m_\psi^2+p_2^2}\right)^2-(p_1+p_2)^2,\\s_{\rm max}&=\left(\sqrt{m_\chi^2+p_1^2}+\sqrt{m_\psi^2+p_2^2}\right)^2-(p_1-p_2)^2.\end{aligned} \tag{A8}$$

The integral is

$$\begin{aligned}\int_{s_{\rm min}}^{s_{\rm max}}f(s)\Theta(s-m_\psi^2)=&F(s)|_{m_\psi^2}^{s_{\rm max}}\Theta(s_{\rm max}-m_\psi^2)\\&-F(s)|_{m_\psi^2}^{s_{\rm min}}\Theta(s_{\rm min}-m_\psi^2),\end{aligned} \tag{A9}$$

with $F(s)=\int(s^n-m_\psi^2s^{n-1})ds$. In the low temperature limit, we can assume m_ψ^2 is close to $s_{\rm max}$, so the second term is negligible. This was also verified with a numerical calculation of the second term. We can solve this integral for the simple $n=l=0$ case step by step. First,

$$F(s)|_{m_\psi^2}^{s_{\max}} = -m_\psi^2 + s_{\max} - m_\psi^2 \log\left(\frac{s_{\max}}{m_\psi^2}\right) \simeq \frac{(s_{\max} - m_\psi^2)^2}{2m_\psi^2}, \tag{A10}$$

where we consider only the leading order in $s_{\max} - m_\psi^2$. (The $n > 0$ cases are even simpler because we can proceed without the last Taylor expansion). Now we solve the p_2 integral, finding eventually a single integral over p_1,

$$n_\phi^{\rm eq} n_\chi \langle \sigma v \cdot E \rangle_{\chi\to\psi} = \frac{g_\chi g_\phi g_\psi g_\phi c_{nl}}{16(2\pi)^5} \int_0^\infty \frac{4T^3 p_1 \left(m_2^2 + 2p_1\left(p_1 + \sqrt{m_2^2 + p_1^2}\right)\right)}{m_1^2} e^{-\frac{(m_\psi^2 - m_\chi^2)}{2Tm_\chi^2}\left(\sqrt{m_2^2+p_1^2} - p_1\right) - \frac{1}{T_2}\sqrt{m_2^2+p_1^2}} dp_1. \tag{A11}$$

In general, solving this integral analytically is challenging. However, we can get sufficiently close by using a saddle-point approximation on the integrand. As result we finally find

$$n_\phi^{\rm eq} n_\chi \langle \sigma v \cdot E \rangle_{\chi\to\psi}(T, T_2) \propto e^{-\frac{(T(m_\chi^2(T-T_2)+m_\psi^2 T_2))^{1/2}}{TT_2}}. \tag{A12}$$

This outcome agrees with the numerical calculation of the integral above. For small values of Δ, we can further simplify $\langle \sigma v \cdot E \rangle_{\chi\to\psi} \propto e^{-\Delta x}$ where $x = \frac{m_\chi}{T}$. We can also see that the result we found above can produce the forward reaction energy transfer $\langle \sigma v \cdot E \rangle_{\psi\to\chi}$ using detailed balance,

$$\langle \sigma v \cdot E \rangle_{\psi\to\chi}(T) = \epsilon^2 \left(\frac{m_\psi^4 - m_\chi^4}{T m_\psi^4} + \frac{3m_\psi^4 + 6m_\chi^2 m_\psi^2 - m_\chi^4}{m_\psi^5}\right) \simeq \frac{\epsilon^2}{m_\chi}\left(1 + \frac{\Delta x}{2}\right), \tag{A13}$$

assuming large x and small Δ, with $\epsilon^2 = \frac{g_\psi g_\phi c_{nl}}{128\pi}$. A direct calculation of the forward reaction energy transfer under the same assumptions verifies this result. With a similar approach, we can calculate the forward reaction cross-section under the same assumptions to obtain

$$\langle \sigma v \rangle_{\psi\to\chi} \simeq \frac{\epsilon^2}{m_\chi^2}\left(1 + \frac{\Delta x}{2}\right). \tag{A14}$$

In solving the coupled Boltzmann equations presented in Eqs. (3) and (4) we use the full results as in Eqs. (A12) and (A13). However, the leading order in Δx, presented in Eqs. (8) and (9), is sufficient to understand the roles the parameters play and yields similar results.

APPENDIX B: KINETIC DECOUPLING AND APPROXIMATE ANALYTIC SOLUTION

The relic density of iELDER DM is determined by the time of kinetic decoupling from the SM bath. In this appendix we derive an analytic approximation for the relevant timescales, following the method of Ref. [12]. Using the results of Appendix A, and working under the same assumptions, Eq. (4) may be rewritten as a differential equation for the bath temperature T and the dark-sector temperature T_χ,

$$\frac{dx_\chi}{dx} = \frac{3}{x} + a e^{-\Delta x}\frac{x - x_\chi}{x}, \tag{B1}$$

where $x_\chi = m_\chi/T_\chi$ and

$$a = \frac{\zeta(3)\Delta m_\chi \epsilon^2}{16\pi^3 H|_{T=m_\chi}}. \tag{B2}$$

The right-hand side of Eq. (B1) contains two competing terms. The first term arises from cannibalization and tends to increase the dark temperature relative to the bath, while the second term comes from the DM-bath interactions and pushes $x_\chi \to x$. The latter falls faster with temperature, and at some point will be too small to compete. At that time, χ will thermally decouple from the bath and begin to cannibalize. This occurs roughly when the second term is of order one, providing an analytical approximation for decoupling,

$$x_d \sim \Delta^{-1} \log a\Delta. \tag{B3}$$

After decoupling, the second term may be ignored, and T_χ grows logarithmically relative to the bath temperature,

$$x_\chi \simeq x_d\left(1 + \frac{3}{x_d}\log\frac{x}{x_d}\right). \tag{B4}$$

Finally, in the iELDER scenario, freeze out of the number density occurs after decoupling of the $3 \to 2$ self-annihilations. Assuming instantaneous freeze out, this happens

when $n_\chi^2\langle\sigma v^2\rangle_{3\to2} \simeq H$, leading to the estimated time of freeze out,

$$(x_\chi)_f \sim \frac{3}{2}\log\frac{\alpha}{3\pi} + \frac{1}{2}\log\frac{m_\chi}{H|_{T=m_\chi}} + \log x_f, \quad \text{(B5)}$$

which relates the temperatures of the bath and of the dark sector at the time of freeze out. Combining Eqs. (B4) and (B5), one can obtain both x_f and $(x_\chi)_f$. (The corresponding approximation for the freeze out temperature in the coscattering scenario can be found in Ref. [11].)

[1] B. W. Lee and S. Weinberg, Cosmological lower bound on heavy neutrino masses, Phys. Rev. Lett. **39**, 165 (1977).
[2] K. Griest and D. Seckel, Three exceptions in the calculation of relic abundances, Phys. Rev. D **43**, 3191 (1991).
[3] E. D. Carlson, M. E. Machacek, and L. J. Hall, Self-interacting dark matter, Astrophys. J. **398**, 43 (1992).
[4] L. J. Hall, K. Jedamzik, J. March-Russell, and S. M. West, Freeze-in production of FIMP dark matter, J. High Energy Phys. 03 (2010) 080.
[5] Y. Hochberg, E. Kuflik, T. Volansky, and J. G. Wacker, Mechanism for thermal relic dark matter of strongly interacting massive particles, Phys. Rev. Lett. **113**, 171301 (2014).
[6] Y. Hochberg, E. Kuflik, H. Murayama, T. Volansky, and J. G. Wacker, Model for thermal relic dark matter of strongly interacting massive particles, Phys. Rev. Lett. **115**, 021301 (2015).
[7] R. T. D'Agnolo and J. T. Ruderman, Light dark matter from forbidden channels, Phys. Rev. Lett. **115**, 061301 (2015).
[8] E. Kuflik, M. Perelstein, N. R.-L. Lorier, and Y.-D. Tsai, Elastically decoupling dark matter, Phys. Rev. Lett. **116**, 221302 (2016).
[9] J. Kopp, J. Liu, T. R. Slatyer, X.-P. Wang, and W. Xue, Impeded dark matter, J. High Energy Phys. 12 (2016) 033.
[10] A. Soni and Y. Zhang, Hidden SU(N) glueball dark matter, Phys. Rev. D **93**, 115025 (2016).
[11] R. T. D'Agnolo, D. Pappadopulo, and J. T. Ruderman, Fourth exception in the calculation of relic abundances, Phys. Rev. Lett. **119**, 061102 (2017).
[12] E. Kuflik, M. Perelstein, N. R.-L. Lorier, and Y.-D. Tsai, Phenomenology of ELDER dark matter, J. High Energy Phys. 08 (2017) 078.
[13] R. T. D'Agnolo, D. Pappadopulo, J. T. Ruderman, and P.-J. Wang, Thermal relic targets with exponentially small couplings, Phys. Rev. Lett. **124**, 151801 (2020).
[14] H. Kim and E. Kuflik, Superheavy thermal dark matter, Phys. Rev. Lett. **123**, 191801 (2019).
[15] R. Frumkin, E. Kuflik, I. Lavie, and T. Silverwater, Roadmap to thermal dark matter beyond the weakly interacting dark matter unitarity bound, Phys. Rev. Lett. **130**, 171001 (2023).
[16] R. Frumkin, Y. Hochberg, E. Kuflik, and H. Murayama, Thermal dark matter from freeze-out of inverse decays, Phys. Rev. Lett. **130**, 121001 (2023).
[17] R. Frumkin, Y. Hochberg, E. Kuflik, and H. Murayama, Phases of dark matter from inverse decays, Phys. Rev. D **112**, 035025 (2025).
[18] M. Battaglieri *et al.*, US cosmic visions: New ideas in dark matter 2017: Community report, in U.S. Cosmic Visions: New Ideas in Dark Matter (2017), arXiv:1707.04591.
[19] P. Asadi *et al.*, Early-universe model building, arXiv:2203.06680.
[20] Y. Hochberg, E. Kuflik, and H. Murayama, Simp spectroscopy, J. High Energy Phys. 05 (2016) 090.
[21] J. Wess and B. Zumino, Consequences of anomalous ward identities, Phys. Lett. **37B**, 95 (1971).
[22] E. Witten, Global aspects of current algebra, Nucl. Phys. **B223**, 422 (1983).
[23] E. Witten, Current algebra, baryons, and quark confinement, Nucl. Phys. **B223**, 433 (1983).
[24] M. E. Peskin, The alignment of the vacuum in theories of technicolor, Nucl. Phys. **B175**, 197 (1980).
[25] J. Preskill, Subgroup alignment in hypercolor theories, Nucl. Phys. **B177**, 21 (1981).
[26] D. A. Kosower, Symmetry-breaking patterns in pseudoreal and real gauge theories, Phys. Lett. **144B**, 215 (1984).
[27] S. Kulkarni, A. Maas, S. Mee, M. Nikolic, J. Pradler, and F. Zierler, Low-energy effective description of dark $Sp(4)$ theories, SciPost Phys. **14**, 044 (2023).
[28] H. M. Lee and M.-S. Seo, Communication with simp dark mesons via z'-portal, Phys. Lett. B **748**, 316 (2015).
[29] A. Hook, E. Izaguirre, and J. G. Wacker, Model independent bounds on kinetic mixing, Adv. High Energy Phys. **2011**, 859762 (2011).
[30] M. Rocha, A. H. G. Peter, J. S. Bullock, M. Kaplinghat, S. Garrison-Kimmel, J. Onorbe, and L. A. Moustakas, Cosmological simulations with self-interacting dark matter I: Constant density cores and substructure, Mon. Not. R. Astron. Soc. **430**, 81 (2013).
[31] A. H. G. Peter, M. Rocha, J. S. Bullock, and M. Kaplinghat, Cosmological simulations with self-interacting dark matter II: Halo shapes vs. observations, Mon. Not. R. Astron. Soc. **430**, 105 (2013).
[32] K. E. Andrade, J. Fuson, S. Gad-Nasr, D. Kong, Q. Minor, M. G. Roberts, and M. Kaplinghat, A stringent upper limit on dark matter self-interaction cross-section from cluster strong lensing, Mon. Not. R. Astron. Soc. **510**, 54 (2021).
[33] X. Shen, T. Brinckmann, D. Rapetti, M. Vogelsberger, A. Mantz, J. Zavala, and S. W. Allen, X-ray morphology of cluster-mass haloes in self-interacting dark matter, Mon. Not. R. Astron. Soc. **516**, 1302 (2022).
[34] D. Eckert, S. Ettori, A. Robertson, R. Massey, E. Pointecouteau, D. Harvey, and I. G. McCarthy, Constraints on dark matter self-interaction from the internal density

profiles of X-COP galaxy clusters, Astron. Astrophys. **666**, A41 (2022).
[35] D. Gilman, Y.-M. Zhong, and J. Bovy, Constraining resonant dark matter self-interactions with strong gravitational lenses, Phys. Rev. D **107**, 103008 (2023).
[36] S. Tulin and H.-B. Yu, Dark matter self-interactions and small scale structure, Phys. Rep. **730**, 1 (2018).
[37] Y. Dengler, A. Maas, and F. Zierler, Scattering of dark pions in Sp(4) gauge theory, Phys. Rev. D **110**, 054513 (2024).
[38] G. Krnjaic *et al.*, A snowmass whitepaper: Dark matter production at intensity-frontier experiments, arXiv:2207.00597.
[39] Y.-D. Tsai, P. deNiverville, and M. X. Liu, Dark photon and muon $g-2$ inspired inelastic dark matter models at the high-energy intensity frontier, Phys. Rev. Lett. **126**, 181801 (2021).
[40] J. R. Jordan, Y. Kahn, G. Krnjaic, M. Moschella, and J. Spitz, Signatures of pseudo-dirac dark matter at high-intensity neutrino experiments, Phys. Rev. D **98**, 075020 (2018).
[41] A. Berlin and F. Kling, Inelastic dark matter at the LHC lifetime frontier: ATLAS, CMS, LHCB, CODEX-b, FASER, and MATHUSLA, Phys. Rev. D **99**, 015021 (2019).
[42] E. Izaguirre, Y. Kahn, G. Krnjaic, and M. Moschella, Testing light dark matter coannihilation with fixed-target experiments, Phys. Rev. D **96**, 055007 (2017).
[43] A. Berlin, S. Gori, P. Schuster, and N. Toro, Dark sectors at the Fermilab seaquest experiment, Phys. Rev. D **98**, 035011 (2018).
[44] M. Toups *et al.*, PIP2-BD: GeV proton beam dump at Fermilab's PIP-II Linac, in Snowmass 2021 (2022), arXiv:2203.08079.
[45] B. Batell, J. Berger, L. Darmé, and C. Frugiuele, Inelastic dark matter at the Fermilab short baseline neutrino program, Phys. Rev. D **104**, 075026 (2021).
[46] M. Duerr, T. Ferber, C. Hearty, F. Kahlhoefer, K. Schmidt-Hoberg, and P. Tunney, Invisible and displaced dark matter signatures at Belle II, J. High Energy Phys. 02 (2020) 039.